Design and Demonstration of a 400 Gb/s Indoor Optical Wireless Communications Link

Ariel Gomez, Kai Shi, Crisanto Quintana, Robert Maher, Grahame Faulkner, Polina Bayvel, *Fellow IEEE,* Benn C. Thomsen, *Member IEEE,* and Dominic O'Brien, *Member, IEEE*

***Abstract*—In this paper we report an ultrafast transparent fibre-wireless-fibre link for indoor optical wireless communications. The link operates over ~3 m range at 416 Gb/s and 208 Gb/s with a wide field of view (FOV) of 40° and 60°, respectively. The system design is fully characterized in simulations, which are in good agreement with the experimental data. To the best of our knowledge, this is the fastest demonstration of an indoor wireless link that offers practical room-scale coverage.**

***Index Terms*—Beam steering, spatial light modulator, optical wireless communication, wavelength division multiplexing, optical fiber communication**

I. Introduction

Optical fibre technologies have allowed Terabit data rates to become widely used in wired communication networks. The recent expansion of optical networks within cities [1], [2] has allowed these rates to be delivered to users' premises. To harness this capability, radio-over-fibre technologies have been developed [3], but these require interfaces to convert from the optical to electrical domain.

An all optical approach is proposed here where the wireless signal is kept in the optical domain and fibre-based transceivers are used at both ends of the wireless link. The corresponding fibre-wireless-fibre (FWF) link is transparent, i.e. independent of the data rate and modulation format. For this geometry, Terabit data rates have already been shown at a short range of ~ 1m and a limited field-of-view (FOV) of < 0.5° [4], [5]. Other work has focused on enhancing the FOV for this type of links with some success [6], [7]. In order to achieve both ultrafast and wide FOV links, narrow beam indoor wireless communication has been proposed [8]–[10]. This approach allows for maximum optical power transfer from the transmitter to the receiver, whilst still satisfying eye-safety constraints. For FWF geometries using narrow beam links, beamsteering capabilities at both transceivers would typically be required if a wide FOV system is targeted. This is due to the fibre-based transceivers having a limited FOV of fractions of a degree [11], thus requiring some form of active alignment via beamsteering [12].

Beamsteering for ultrafast wireless communications has been extensively proposed and demonstrated using actuated mirrors, spatial light modulators (SLMs) and diffraction gratings with tunable lasers [13]–[16]. However, the beamsteering power is limited by the device's steering range and active area. Thus, the addition of passive angle magnification (AM) modules to enhance the overall link FOV is of great advantage as reported in [17].This AM modules allowed for the demonstration of the fastest optical wireless link with practical room-scale coverage at data rates above 100 Gb/s with a FOV of 60°.

In this paper, we report doubling this data rate record using the same FWF link. Optimized wavelength division multiplexing (WDM) techniques and digital coherent transmission are used to demonstrate 418 Gb/s (14 channels x 29.9 Gb/s/channel) and 209 Gb/s (7 channels x 29.9 Gb/s/channel) with a wide FOV of 40° and 60°, respectively, at a range of ~3 m. The multiple WDM channels are kept as a single beam under free space propagation, given the compact Nyquist-WDM channel separation that minimized the SLM dispersive effects.

A full FWF link design is given here, with new detailed theoretical analysis. The optical loss trade-off between the beamsteering power and required link FOV is quantitatively shown. The predominant loss factor is found to be vignetting at the receiver due to beam divergence under free space propagation. These results can be generalized to other narrow beam indoor optical wireless architectures requiring active beamsteering and angle magnification.

The rest of this paper is arranged as follows: section II describes the free space link design; section III gives the link characterization for a continuous wave experiment; section IV defines the transmission system and shows the

The research is funded by the UK Engineering and Physical Sciences Research Council (EPSRC) under grants EP/J008842/1 (COMIMO project) and 1181352 (Future Optical Wireless Communications).

Ariel Gomez, Crisanto Quintana, Grahame Faulkner, and Dominic O'Brien are with the Department of Engineering Science, University of Oxford, Oxford OX13PJ, UK. (e-mail: ariel.gomezdiaz@eng.ox.ac.uk; crisanto.quintanasanchez@eng.ox.ac.uk; grahame.faulkner@eng.ox.ac.uk; dominic.obrien@eng.ox.ac.uk).

Kai Shi, Robert Maher, Benn C. Thomsen and Polina Bayvel are with the Department of Electronics and Electrical Engineering, University College London, London WC1E 7JE, UK. (e-mail: k.shi@ucl.ac.uk; r.maher@ucl.ac.uk; b.thomsen@ucl.ac.uk; p.bayvel@ucl.ac.uk).

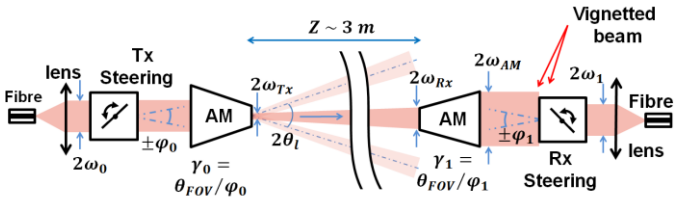

Figure 1. Link model. AM is an angle magnifier and SLM is a spatial light modulator.

experimental results for sub-Terabit data rates; and finally, section V gives the paper conclusions.

II. Free Space Design

Figure 1 shows the link model for narrow beam communications with fibre-based transceivers. The design requires accurate steering devices at both ends to efficiently direct and to couple light back into the receiving fibre. The model includes AM modules to achieve practical indoor coverage with a FOV ≥ ±30° (60° full-cone angle).

The link's detailed optical path is as follows (see Figure 1). Light collimated from an optical fibre illuminates a transmitter (Tx) steering device. The device's effective aperture is $2\omega_0$ and the steering capability is $\pm\varphi_0$. The steered light enters an AM module enhancing the link FOV θ_{FOV} by a factor of $\gamma_0 = \theta_{FOV}/\varphi_0$. The output beam at the Tx with width ω_{Tx} then propagates in free space for a distance $Z \sim 3$ m, whilst experiencing beam spreading due to the inherent diffraction of light. The beam width at the receiver aperture becomes ω_{Rx}. Using classical Gaussian beam propagation theory, and assuming the beam waist at the Tx aperture, it can be shown that,

$$\omega_{Rx} = \omega_{Tx}\sqrt{1 + (Z/Z_{Tx})^2}\,; \qquad Z_{Tx} = \pi\omega_{Tx}^2/\lambda \tag{1}$$

Where Z_{Tx} is the Rayleigh length of the Gaussian beam and λ is the wavelength of operation. After the receiver (Rx) aperture, a second AM de-magnifies the beam angle by

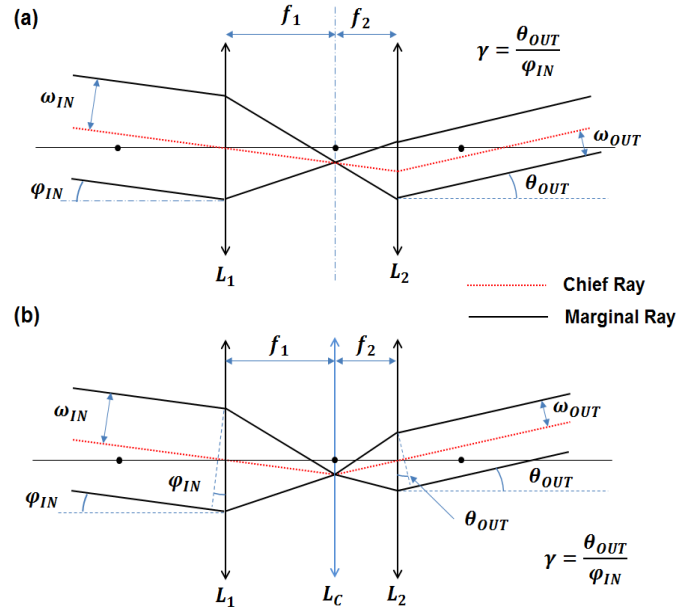

Figure 2. AM afocal system with magnification $\gamma = \theta_{OUT}/\varphi_{IN}$ for (a) a simple two-lens configuration and (b) a 3-lens setup using a field lens L_C.

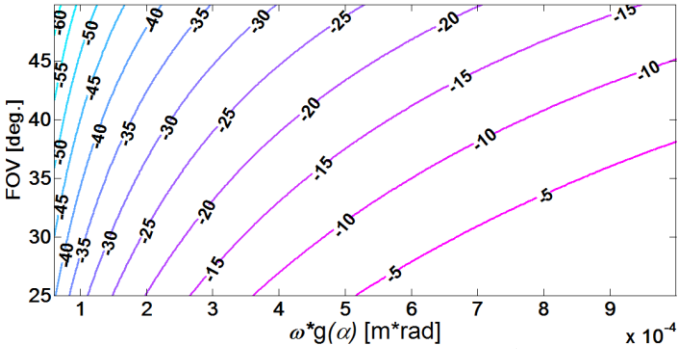

Figure 3. Characteristic loss for a symmetric link $\mathcal{L}_{V,SL}$ and free space range of $Z = 3$ m. The contour lines represent the loss levels as a function of the FOV and the product $\omega \cdot g(\alpha)$. Here ω and α are the steering device's aperture radius and steering range, respectively. The definition of function g is given in equation (3).

$\gamma_1 = \theta_{FOV}/\varphi_1$ where $\pm\varphi_1$ is the Rx steerer device range. Simultaneously, the beam width is magnified to ω_{AM} due to etendue conservation in passive optical systems [18]. This effect creates a geometric loss $\mathcal{L}_V$, due to vignetting in the Rx steerer with aperture size ω_1 if $\omega_{AM} > \omega_1$. Finally, the beam is coupled back into an optical fibre with coupling loss $\mathcal{L}_F$.

In the next sections, a theoretical model for the AM is developed. This model is then used to estimate the link's geometric loss $\mathcal{L}_V$ for various scenarios. Finally, the coupling loss $\mathcal{L}_F$ is simulated for a single mode fibre (SMF)-based receiver using the ray tracing engine Zemax.

A. Angle Magnification

A basic magnification module is given by a two-lens optical arrangement as shown in Figure 2 (a). This is an afocal setup where lenses L_1 and L_2 share the intermediate focal plane. A modified configuration is introduced here, which includes a field lens L_C located in this intermediate plane. Figure 2 (b) shows the modified ray tracing layout. Lens L_C images L_1's aperture onto L_2's. This centers the incoming beam footprint on lens L_2, thus reducing geometrical aberrations. Using basic imaging and trigonometric arguments, it is obtained:

$$\frac{1}{f_1} + \frac{1}{f_2} = \frac{1}{f_C}; \quad \frac{f_2}{f_1} = \frac{\omega_{OUT}/\cos\theta_{OUT}}{\omega_{IN}/\cos\varphi_{IN}} = \frac{\tan\varphi_{IN}}{\tan\theta_{OUT}} \tag{2}$$

From equation (2) the following important condition it can be deduced:

$$\omega_{OUT} \cdot g(\theta_{OUT}) = \omega_{IN} \cdot g(\varphi_{IN})\,; \; with\; g(\alpha) = \tan\alpha/\cos\alpha \tag{3}$$

Equation (3) gives a conservation of the product $\omega \cdot g(\alpha) = constant$. Thus, for small $\theta_{OUT}, \varphi_{IN}$ an angular magnification of $\gamma = \theta_{OUT}/\varphi_{IN}$ implies a beam width de-magnification of $\omega_{OUT}/\omega_{IN} = 1/\gamma$. The implications of this beam width reduction to increase the link's FOV are not straightforward, and will be studied in the next section as part of the geometric loss model.

B. Geometric loss model

The downlink (DL) is shown in Figure 1. As described in the introduction of section II, the beam is collimated, accurately steered and magnified using an AM to achieve a wide angle θ_{FOV}. In free space, the beam expands under

Gaussian propagation to be later collected by the receiver aperture. A second AM scales the link angle down to the Rx steering device range. In doing so, a geometric loss $\mathcal{L}_{V,DL} = (\omega_1/\omega_{AM})^2$ occurs if $\omega_{AM} > \omega_1$ due to vignetting. Following the downlink's optical path, and using equations (1) and (3), $\mathcal{L}_{V,DL}$ becomes,

$$\mathcal{L}_{V,DL} = 10\,log_{10}(\mathcal{E}_{Tx} \cdot \mathcal{E}_{Rx}) - 10\,log_{10}(\mathcal{E}_{Tx}^2 + \lambda^2 Z^2\, g^4(\theta_{FOV}))$$
$$\mathcal{E}_{Tx} = \pi\omega_0^2\, g^2(\varphi_0) = \pi\omega_{Tx}^2\, g^2(\theta_{FOV}) \quad (4)$$
$$\mathcal{E}_{Rx} = \pi\omega_1^2\, g^2(\varphi_1) = \pi\omega_{Rx}^2\, g^2(\theta_{FOV})$$

For the uplink (UL) a similar condition vignetting effect occurs, but this time the Tx steering device is the aperture stop with the vignetting loss given by $\mathcal{L}_{V,UL} = (\omega_0/\omega_{AM})^2$. It can be easily deduced from equation (4) that,

$$\mathcal{L}_{V,UL} = 10\,log_{10}(\mathcal{E}_{Tx} \cdot \mathcal{E}_{Rx}) - 10\,log_{10}(\mathcal{E}_{Rx}^2 + \lambda^2 Z^2\, g^4(\theta_{FOV})) \quad (5)$$

Where $\mathcal{E}_{Tx}$ and $\mathcal{E}_{Rx}$ are the same as before. For a symmetric link (SL) where $\mathcal{E}_{Tx} = \mathcal{E}_{Rx}$, the bidirectional characteristic link loss can be defined as $\mathcal{L}_{V,SL} = \mathcal{L}_{V,DL} = \mathcal{L}_{V,UL}$. Figure 3 shows the $\mathcal{L}_{V,SL}$ levels as a function of the FOV and steering device's capability defined by equation (3). The free space range is $Z = 3$ m. It can be seen that for $\omega \cdot g(\alpha) < 3 \cdot 10^{-4}\, m \cdot rad$ the loss $\mathcal{L}_{V,SL}$ drastically increases beyond 25 dB. The FOV is also a critical factor. For instance, when $\omega \cdot g(\alpha) = 2 \cdot 10^{-4}\, m \cdot rad$, $\mathcal{L}_{V,SL}$ rises by 10 dB when the link's FOV increases from 30° to 45°. This outlines the challenge of designing a functional bidirectional link as the coverage is increased.

For the rest of the paper, a symmetric link with identical Tx and Rx steering modules is studied. This restriction is imposed by the availability of steering devices at the time of the experiments. For a general case, equations (4) and (5) can be used to design an asymmetric link.

C. Steering and aberration study

In this section the transceiver performance is studied (fibre coupling, beamsteering and AM given in Figure 1) using Zemax ray tracing software. For the steering device, SLMs are used to achieve not only the beamsteering function but also to correct for geometric aberrations introduced by the AM system. This adaptive optics capability is particularly important for wide FOV SMF-based transceivers as will be shown here.

First, the AM is designed based on the available steering module. Then, the overall transceiver function is simulated.

1) AM design

The AM angular magnification $\gamma = \theta_{OUT}/\varphi_{IN}$ is determined by the SLM beamsteering range and the target FOV. The SLM in use is a 512 x 512 pixels device (BNS HSP512-1550) with a pixel size of $p = 15\,\mu m$. The phase modulation per pixel is 2π at the optimized wavelength of $\lambda = 1550\,nm$. This gives a beamsteering range of $\varphi_{max} = \lambda/2p \sim \pm 3°$ and the product $\cdot\, g(\alpha) \sim 2 \cdot 10^{-4}\, m \cdot rad$. Using this value, from Figure 3 a target FOV of $\theta_{FOV} = 30°$ is a good compromise between the link coverage and the geometric loss of $\mathcal{L}_V \sim 25$ dB.

The required angular magnification is then $\gamma = \theta_{FOV}/\varphi_{max} = 10$. Using equation (2), an afocal system can be designed with a field lens f_C and $f_1/f_2 = 11$. Figure 4 shows an AM design schematic using off-the-shelve components. The focal length $f_C \sim 7$ mm was chosen from $1/f_C = 1/f_1 + 1/f_2$, with $f_1 = 77$ mm and $f_2 = 8$ mm. All f values are given for $\lambda = 1550$ nm and they are referenced to the back focal plane, i.e. the planar surface of each lens.

2) Ray tracing setup

Zemax was used to characterize the AM as a function of the input field angle as shown in Figure 4. In these simulations, an incoming beam with uniform power and planar wavefront was used. The AM output illuminates an SLM in an off-axis configuration, followed by a collimator focusing the beam onto an SMF fibre facet. The SLM is modelled as a 512 x 512 phase array where the pixilation loss, phase quantization and inter-pixel crosstalk are ignored. Two SLM functions are implemented: beamsteering and defocus. For a beamsteering angle φ_{SLM}, a continuous ramp phase profile is defined as follows:

$$Ramp = \pi\eta r_N$$
$$\eta = \frac{N}{2}\frac{\varphi_{SLM}}{\varphi_{max}} \quad ; \quad \varphi_{max} = \lambda/(2p) \quad (6)$$

Where $N = 512$ is the SLM number of pixels and $r_N = r/(N/2), r = \{-N/2 \ldots N/2 - 1\}$ is the normalized radial pixel coordinate whose origin is at the centre of the SLM. For the defocus function, a 1st order Zernike polynomial was used given by:

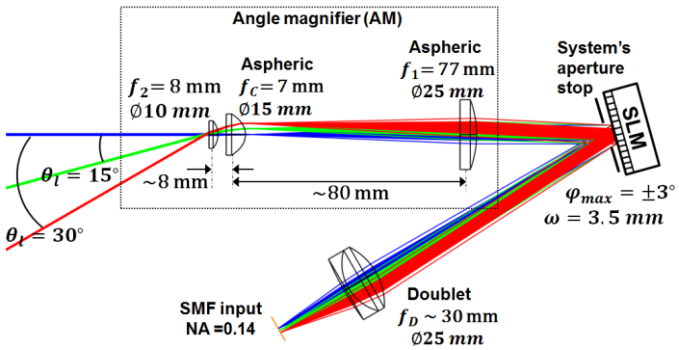

Figure 4. Zemax layout of the ray tracing through the AM, SLM in reflection, and finally a doublet focusing the light onto the SMF input facet. There are three angular field present: 0° (blue rays), 15° and 30°. For visualization purposes, the phase grating on the SLM is fixed for the 0° field.

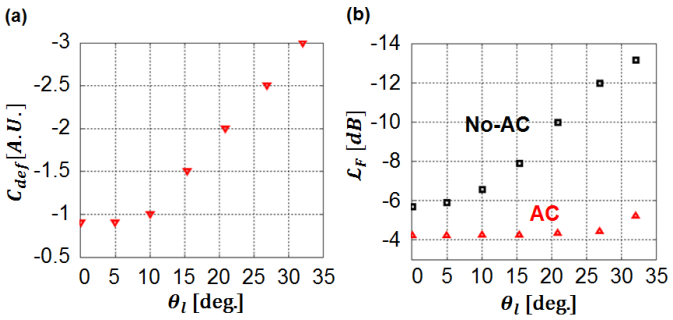

Figure 5. Zemax simulation results: (a) the defocus coefficient C_{def} as a function of θ_I (b) the fibre coupling loss $\mathcal{L}_F$ as a function of θ_I. AC means aberration correction.

$$Z_{power} = C_{def} \cdot \sqrt{3} \cdot (2r_N^2 - 1) \quad (7)$$

Where C_{def} is a defocus coefficient..

3) Simulation results

The SLM beamsteering and defocus phase profiles were optimized to maximize the power coupling into the SMF fibre as a function of the link angle θ_l. The SMF fibre has a numerical aperture NA = 0.14. The coupling loss $\mathcal{L}_F$ is numerically determined in Zemax using the normalized overlap integral between the fibre and wavefront amplitude. This is a measure of aberrations in the optical system [19].

The simulation results showed that the AM was able to magnify to $\theta_l > 30°$. Geometrical aberrations were corrected applying defocus profiles as those given by equation (7). The corresponding optimized defocus coefficient C_{def} are shown in Figure 5 (a). This correction was necessary not only to keep the receiving fibre coupling loss $\mathcal{L}_F$ under control (see Figure 5 (b)) but also to perform beam shaping of the output beam at the transmitter.

In a symmetric FWF system, the transmitted narrow beam will suffer from beam spreading due to aberrations added by the Tx AM. Thus, pre-compensation for aberrations will also be needed at the Tx. This will be verified in the following experimental sections.

III. Link Characterization

A symmetric FWF link was built based on the design given in Figure 4. A picture of the SMF-based transceivers is shown in Figure 6. Polarization optics (PO) is used to set the illumination beam on the SLM as vertically polarized. This allows the pixel modulation to be phase-only.

The FWF link was characterized in a setup similar to Figure 1 as a function of the link angle θ_l. The Tx was connected to a 1550 nm laser source and the Rx fibre was monitored using an optical power meter. In this section, the beam divergence was initially studied due to diffraction as well as the beam spreading due to aberrations. Then, the link FOV was estimated for the SLM steering range combined with the required correction for aberrations. Finally, the link loss was calculated as a function of θ_l comparing it with the theoretical predictions.

A. Free space propagation

After the Tx, an InGaAs camera recorded the beam transverse profile when varying the free space propagation

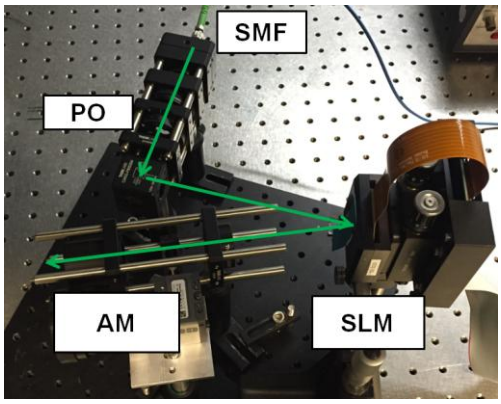

Figure 6. Picture of the Tx / Rx transceiver. PO means polarization optics.

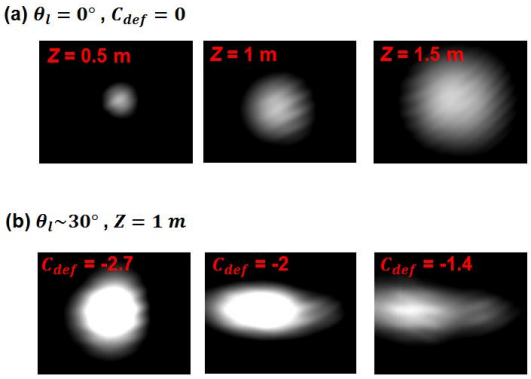

Figure 7. Beam propagation study for (a) small θ_l~0 and variable free space distance Z and (b) large θ_l~30° and variable defocus correction C_{def}.

distance Z. The results are given in Figure 7 (a) for θ_l~0°, i.e. negligible geometric aberrations. The beam diffracts keeping an approximately Gaussian profile as it propagates with a measured divergence angle of $\vartheta_{div} = 0.06°$. Theoretically, the divergence from the equation (1) can also be estimated for $Z \gg Z_{Tx}$ as follows:

$$\vartheta_{div}^0 \sim \frac{\lambda}{\pi \omega_{Tx}} \quad (8)$$

Where ω_{Tx} is the beam waist of the Gaussian beam in free space located just after the Tx AM output. Using equation (3) $\omega_{OUT} = \omega_{Tx} = 0.55$ mm is obtained for an AM with $\gamma = 10$ and an input beam width $\omega_{IN} = \omega_{SLM} \sim 3.5$ mm specified by the Thorlabs F810APC-1550 collimator. Then, substituting in equation (8) $\vartheta_{div}^0 = 0.05°$ is obtained. This theoretical value is in agreement with the experimental $\vartheta_{div} = 0.06°$, the latter being slightly higher due to either AM misalignment or other geometrical distortions in the system.

For large θ_l, beam distortions in the AM are also a major factor in the spreading of the beam under propagation.

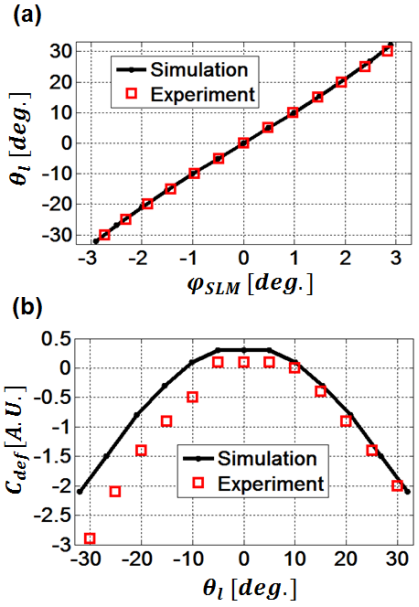

Figure 8. Link characterization: (a) link angle as a function of the SLM steering φ_{SLM}; (b) optimum defocus coefficient C_{def} as a function of the link angle θ_l.

Corrections for geometrical aberrations are required to keep an approximate Gaussian beam shape. Figure 7 (b) shows the beam's transverse profile for θ_l~30° after Z = 1 m. It can be seen that, unless the optimum defocus profile with $C_{def} = -2.7$ is added to the SLM, the beam energy quickly disperses. The consequences at the design distance Z = 3 m are such that no optical power is detected at the Rx fibre for large link angles.

B. Link FOV with aberration correction

The experimental link FOV as a function of the SLM steering θ_{SLM} is shown in Figure 8 (a). The simulation and experimental curves coincide following an angular magnification $\gamma = 10$ performed by the designed AM. The trend is quasi linear. The deviation from a perfectly linear performance is due to the AM not having ideal thin lens components, thus the lenses' focal lengths slightly vary as a function of θ_l.

Additionally, to keep a narrow beam during the free space propagation, defocus profiles are added to the SLM default ramp steering function. Figure 8 (b) gives the defocus coefficient C_{def} as a function θ_l. The theoretical simulations are in agreement with the experimental curves: low angles require a constant defocus profile C_{def}^0, followed by a linear C_{def} increment after $|\theta_l| \geq 10°$. This initial C_{def}^0 varies from setup to setup and it depends on the optical alignment within the AM (relative position of its lenses). It can also be seen that a larger defocus correction is required for a negative θ_l in the experimental curve. This is due to the AM's optical axis being displaced with respect to the SLM's, thus creating some asymmetry (and uneven aberrations) in an otherwise circularly symmetric optical system.

The analysis was carried out for the Tx but it can be extended to the Rx as this FWF link geometry is symmetric.

C. Link loss

The steering modules capabilities have been experimentally characterized as a function of θ_l. The overall link performance will now be considered when two identical transceivers are used at both ends of the SMF-wireless-SMF geometry. The link alignment for each θ_l is performed by rotating the transceivers whilst keeping the free space distance at Z~3 m. The detailed procedure for automated tracking and localization is explained elsewhere, with a latency of the order of seconds [12].

Once the alignment is carried out, the total link loss Γ can be estimated as a function of θ_l. Figure 9 shows the corresponding experimental results as well as the simulated loss curves for different aberration correction (AC) implementations. The link loss Γ can be separated in the following components:

$$\Gamma(\theta_l) = \mathcal{L}_V + \mathcal{L}_F(\theta_l) + \mathcal{L}_{SLM}(\theta_l) + \mathcal{L}_O \quad (9)$$

Where $\mathcal{L}_V$, $\mathcal{L}_F$ and $\mathcal{L}_{SLM}$ are the vignetting, fibre coupling and SLM loss, respectively. $\mathcal{L}_O$ refers to other sources of loss not included here such as reflection or scattering loss from the optical components. $\mathcal{L}_V$ = -25 dB is the predominant loss factor as predicted in section II.B, which is also independent of θ_l. $\mathcal{L}_{SLM}$ is the $sinc^2$ loss due to the pixelated nature of the SLM. This amounts to a maximum of 4 dB at the steering range limit [20].

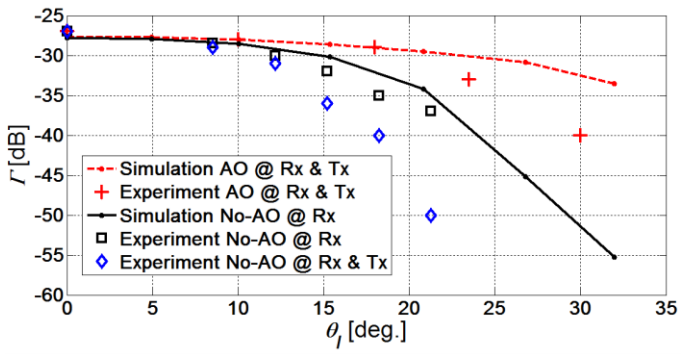

Figure 9. Link loss characterization. The experiment and simulation data is displayed for different aberration correction (AC) scenarios.

From Figure 9, there is a good agreement (within ±3 dB) between the experimental and simulation curves for $\theta_l \leq 20°$. However, the simulation underestimates the coupling loss for $\theta_l > 20°$. This is possibly due to the Zemax phase array model overcorrecting for aberrations.

Finally, the importance of AC was experimentally verified in an SMF-wireless-SMF link with large FOV. The system with no AC at the Tx nor the receiver suffers from exponential loss for $\theta_l > 10°$. When no AC is applied to the receiver, the additional loss becomes considerable for $\theta_l > 20°$. AC at both terminals gives the best performance. However, a link budget reduction of $\Delta\Gamma$ = 13 dB is obtained when θ_l increases from 0° to 30°. This justifies the use of SLMs instead of more conventional steering devices with no AC capability.

D. WDM capabilities

The SMF-wireless-SMF link geometry is compatible with fibre communication transmission systems. WDM capabilities are also desirable to linearly increase the free space link data rates. However, given the SLM-based transceivers, the beamsteering action is a function of the wavelength of operation as given by (6). This dispersive effect translates into an additional beam spreading in the Rx plane, which can be significant given the Rx entrance aperture diameter of only 10 mm (see first AM lens in Figure 4).

To quantify the dispersion in the Rx plane, let us assume that an incoming beam with wavelength λ_0 is aligned to this Rx aperture's center. It can be shown that a beam with wavelength λ will experience a beam walk-off ΔS of,

$$\Delta S \sim \theta_l \cdot Z \cdot \Delta\lambda/\lambda_0, \qquad \Delta S \ll Z \quad (10)$$

Where Z is the free space propagation distance from the Tx and $\Delta\lambda = \lambda - \lambda_0$. Therefore, the vignetting loss at the Rx entrance aperture will vary as a function of channel wavelength and the propagation distance, the worst case scenario occurring at $\theta_l = \pm 30°$.

For our system, this is critical at the target distance Z~3 m where the beam footprint diameter fills the receiver entrance aperture due to divergence (see section III.A). It has been experimentally shown that, under these conditions, a detuning of $\Delta\lambda = 2.5\ nm$ contributes to ~ 2 dB vignetting loss [21]. Using (10), this corresponds to $\Delta S = 2.5\ mm$ at $\theta_l = 30°$. Therefore, it is advantageous to have a closely spaced WDM comb to minimize vignetting due to

dispersion. The coupling into Rx fibre is not affected because, for the symmetric link under study, the dispersion caused at the Tx SLM is compensated by the Rx SLM.

IV. Transmission Experiment

In this section, the FWF link is successfully integrated with a state-of-the-art optical digital coherent system. The experimental realization of a wide FOV = ±30° transparent FWF link with a WDM capacity over 200 Gb/s is shown.

A. Coherent WDM system

The FWF link was connected via SMF fibres to an optical digital coherent system as shown in Figure 10. The coherent transmitter is a Nyquist-WDM (N-WDM) transceiver [22] that generates K_{ch} = 1, 7 or 14 WDM channels. Figure 11 (a) and (b) shows the optical spectral comb generated for K_{ch} = 7 and K_{ch} = 14 channels, respectively, with a channel spacing of ~8.2GHz. Only the modulated carriers with peak power higher than −22 dBm were used to homogenize the channel performance. Each channel carried an 8 Gbaud X-quadrature amplitude modulation (X-QAM) signal, with X = {4, 16}. A data rate per channel of 14.95 Gb/s and 29.9 Gb/s was achieved, respectively, assuming a 7% overhead hard decision forward error correction (FEC) [23]. After the coherent transmitter, the N-WDM signal was amplified using a booster EDFA. A variable optical attenuator (VOA) was subsequently used for optical power control.

The modulated light is later fed into the Tx steering to create the wireless link. During free space propagation, the multi-channel narrow beam not only diverges but also disperses. The dispersion is negligible though, due to the compact N-WDM comb of maximum 14 channels with an overall spectrum $\Delta\lambda < 1$ nm. After free space propagation, the WDM beam enters the Rx steering module. The Rx SLM not only compensates for beamsteering and aberrations, but also corrects the Tx SLM channel dispersion, thus allowing dispersion-free coupling into the Rx SMF fibre. An optical EDFA preamplifier follows to improve the receiver sensitivity. A standard coherent receiver with an electrical bandwidth of 63GHz is used to process the N-WDM channels simultaneously. Digital signal processing (DSP) is later applied to the captured waveforms from a 160GSample/s real-time oscilloscopes to recover the Nyquist pulse shaped X-QAM signal [22].

B. X-QAM sensitivity

Back-to-Back (BtoB), through fibre only, experiments were carried out to characterize the receiver sensitivity as

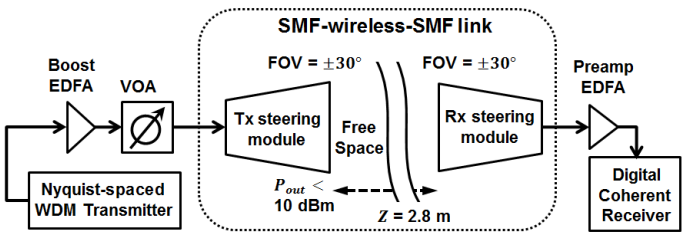

Figure 10. Experimental setup. The transmission system is an extension of the FWF link using SMF fibres. VOA is a variable optical attenuator.

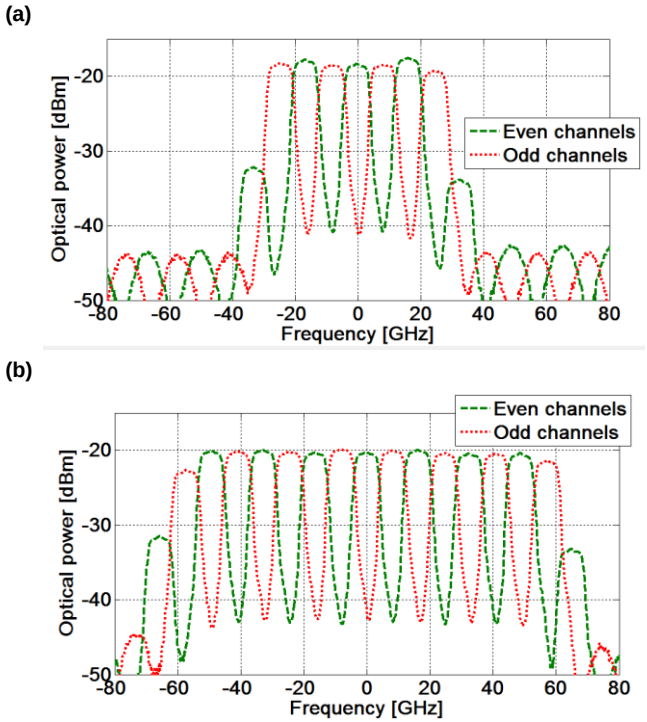

Figure 11. Measured optical spectra at the transmitter for (a) 7 and (b) 15, N-WDM optical comb with a resolution of 0.01 nm. The even and odd carriers are separately modulated. Only the modulated carriers are plotted for a 16-QAM symbol.

function of the Rx input power (just before the EDFA preamplifier). The results are shown in Figure 12 for different X-QAM modulations. Receiver sensitivities (at the FEC limit) of -49 dBm and -42 dBm were obtained for the 4-QAM and 16-QAM modulations, respectively.

As the modulation changes from 4QAM to 16-QAM, there is a measured sensitivity penalty of ~7 dB. This relative drop is as predicted by the theoretical curves, giving a bits per-symbol enhancement factor of 2.

C. Throughput study

For the experiments, the output power after the Tx steering module was initially set to a maximum of 10 dBm to satisfy eye safety constraints [24]. From this point, additional power loss was induced by the VOA. Figure 13 shows the system bit error rate (BER) vs VOA attenuation. The curves are plotted for different modulation formats, number of WDM channels K_{ch} and link angles θ_l.

Using a 7% overhead hard-decision FEC, the link is operational if the BER is lower than $3.8 \cdot 10^{-3}$ [25]. The

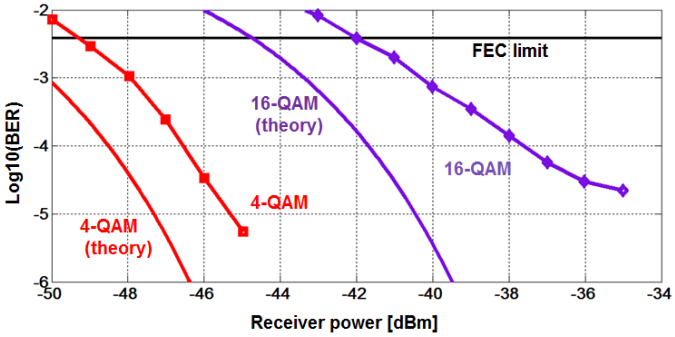

Figure 12. Back-to-back sensitivity curves for different X-QAM modulations. The theoretical curves were taken from [27].

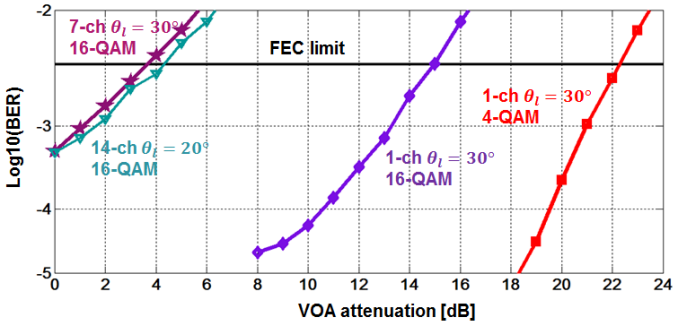

Figure 13. Coherent system performance. The plotted curves are defined by the link angle θ_l, the modulation format and the number of transmitted N-WDM channels. For the 7 and 14 channel results, instead of individual channels, the average BER per channel is given to simplify the plots' visualization.

intersection of the FEC limit with each BER curve indicates the available link margin for that configuration. (As an example, the "1-ch $\theta_l = 30°$ 4 QAM" curve shows that an additional 22 dB of attenuation can be added and the BER remains within acceptable limits).

From the single channel curves in Figure 13, it can be seen that by changing the modulation format from 4-QAM to 16-QAM the link margin was reduced by ~ 7dB. This penalty was expected from Figure 12 due to receiver sensitivity reduction, with the advantage of doubling the data rate per channel. Additionally, for the multi-channel curves, the 10 dBm optical power limit was equally split amongst the beam's K_{ch} channels. Therefore, a link budget penalty per channel of $\log_{10} K_{ch}$ was imposed. The choice of $K_{ch} = 7, 14$ for link angles $\theta_l = 30°, 20°$, respectively, was determined by this penalty, and the link loss Γ as a function of θ_l (see Figure 9).

Therefore, it can be concluded that the FWF link operates at 418 Gb/s (14 x 29.9 Gb/s/channel) and 209 Gb/s (7 x 29.9 Gb/s/channel) assuming a 7% overhead hard-decision FEC with a wide FOV (full-cone) of 40° and 60°, respectively. The hard decision based maximum achievable rates are 445.15 Gb/s and 222.52 Gb/s, which are calculated by using $C = K_{ch} \cdot B \log_2 M \cdot [1 + p \log_2 p + (1-p)\log_2(1-p)]$; where p is the best achievable BER of the system, B is the baudrate and M the modulation order. To the best of our knowledge, this is the fastest demonstration of an indoor wireless link with a FOV that offers practical room-scale coverage, doubling the previous reported throughput for an equivalent link [17].

V. Conclusion

This paper describes the design and characterization of a wide-FOV ultrafast indoor optical wireless link using fibre-based transceivers. Wide area coverage is achieved by combining narrow beams with accurate beamsteering and adaptive optics units at both terminals.

The potential of SMF-wireless-SMF links is shown. We report a record data rate of 418 Gb/s and 209 Gb/s at a FOV of ±20° and ±30°, respectively, at a free space transceiver's distance of 3 m. The optical link is eye safe and potentially bidirectional. As the system design is transparent, then higher data rates and simpler transmission schemes are possible.

Future work includes the demonstration of similar fibre-wireless-fibre links with cost effective steering components and multimode fibres. Point-to-multipoint communications for this type of narrow beam links are currently research topics of interest [26].

Acknoledgement

The authors thank Dr. Tianhua Xu from UCL London for the fruitful discussion on the FEC coding and maximum achievable rate.

References

[1] P. Ödling, T. Magesacher, S. Höst, P. O. Börjesson, M. Berg, E. Ab, and E. Areizaga, "The Fourth Generation Broadband Concept," *Adv. Signal Process. Commun.*, no. January, pp. 63–69, 2009.

[2] M. Maier, M. Lévesque, and L. Ivanescu, "NG-PONs 1&2 and Beyond: The Dawn of the Uber-FiWi Network," *IEEE Netw.*, no. March, pp. 15–21, 2012.

[3] N. Ghazisaidi and M. Maier, "Fiber-Wireless (FiWi) Access Networks: Challenges and Opportunities," *IEEE Netw.*, no. February, pp. 36–42, 2011.

[4] J. Wang, J. Yang, I. M. Fazal, N. Ahmed, Y. Yan, H. Huang, Y. Ren, Y. Yue, S. Dolinar, M. Tur, and A. E. Willner, "Terabit free-space data transmission employing orbital angular momentum multiplexing," *Nat. Photonics*, vol. 6, no. June, 2012.

[5] H. Huang, G. Xie, Y. Yan, N. Ahmed, Y. Ren, Y. Yue, D. Rogawski, M. J. Willner, B. I. Erkmen, K. M. Birnbaum, S. J. Dolinar, M. P. J. Lavery, M. J. Padgett, M. Tur, and A. E. Willner, "100 Tbit/s free-space data link enabled by three-dimensional multiplexing of orbital angular momentum, polarization, and wavelength.," *Opt. Lett.*, vol. 39, no. 2, pp. 197–200, Jan. 2014.

[6] C. W. Oh, F. M. Huijskens, S. Zou, H. Chen, E. Tangdiongga, and A. M. J. Koonen, "36 . 7 Gbps Spectrum-efficient Indoor Optical Wireless System with Beam-Steering," *Proc. ECOC*, vol. We365.

[7] K. Wang, S. Member, A. Nirmalathas, S. Member, C. Lim, and E. Skafidas, "4 x 12 . 5 Gb / s WDM Optical Wireless Communication System for Indoor Applications," *J. Light. Technol.*, vol. 29, no. 13, pp. 1988–1996, 2011.

[8] C. W. Oh, E. Tangdiongga, and a. M. J. Koonen, "Steerable pencil beams for multi-Gbps indoor optical wireless communication," *Opt. Lett.*, vol. 39, no. 18, p. 5427, Sep. 2014.

[9] C. W. Oh, F. M. Huijskens, Z. Cao, E. Tangdiongga, and a M. J. Koonen, "Toward multi-Gbps indoor optical wireless multicasting system employing passive diffractive optics.," *Opt. Lett.*, vol. 39, no. 9, pp. 2622–5, 2014.

[10] K. Wang, A. Nirmalathas, C. Lim, and E. Skafidas, "High-speed indoor optical wireless communication system with single channel imaging receiver," *Opt. Express*, vol. 20, no. 23, p. 25356, Nov. 2012.

[11] A. Gomez, C. Quintana, G. Faulkner, and D. O. Brien, "Challenges in Wide Coverage Indoor Optical Communications Using Fibre-Wireless-Fibre Links for Terabit data rates," *IEEE GlobeCom*, pp. 1–5, 2015.

[12] A. Gomez, K. Shi, C. Quintana, G. Faulkner, B. C. Thomsen, M. Ieee, D. O. Brien, and M. Ieee, "A 50 Gb / s Transparent Indoor Optical Wireless Communications Link with an Integrated Localization and Tracking System," *J. Light. Technol.*, vol. 34, no. 10, pp. 1–8, 2016.

[13] J. Morrison, M. Imboden, T. D. C. Little, and D. J. Bishop, "Electrothermally actuated tip-tilt-piston micromirror with integrated varifocal capability," *Opt. Express*, vol. 23, no. 7, p. 9555, 2015.

[14] J. R. LINDLE, A. T. WATNIK, and V. A. CASSELLA, "Efficient multibeam large-angle nonmechanical laser beam steering from computer-generated holograms rendered on a liquid crystal spatial light modulator," *Appl. Opt.*, vol. 55, no. 16, pp. 4336–4341, 2016.

[15] F. Feng, I. H. White, and T. D. Wilkinson, "Free Space Communications With Beam Steering a Two-Electrode Tapered Laser Diode Using Liquid-Crystal SLM," *J. Light. Technol.*, vol. 31, no. 12, pp. 2001–2007, 2013.

[16] C. W. J. Oh, E. Tangdiongga, and A. M. J. T. Koonen, "42 . 8 Gbit / s Indoor Optical Wireless Communication with 2-Dimensional Optical Beam-steering," in *OFC*, 2015, p. M2F.3.

[17] A. Gomez, K. Shi, C. Quintana, M. Sato, G. Faulkner, B. C. Thomsen, and D. O. Brien, "Beyond 100-Gb / s Indoor Wide Field-of-View Optical Wireless Communications," *Photonics Technol. Lett.*, vol. 27, no. 4, pp. 367–370, 2015.

[18] S. Collins, D. C. O'Brien, and A. Watt, "High gain, wide field of view concentrator for optical communications.," *Opt. Lett.*, vol. 39, no. 7, pp. 1756–9, 2014.

[19] R. E. Wagner and W. J. Tomlinson, "Coupling efficiency of optics in single-mode fiber components.," *Appl. Opt.*, vol. 21, no. 15, pp. 2671–2688, 1982.

[20] M. a Seldowitz, J. P. Allebach, and D. W. Sweeney, "Synthesis of digital holograms by direct binary search.," *Appl. Opt.*, vol. 26, no. 14, pp. 2788–98, 1987.

[21] A. Gomez, C. Quintana, G. Faulkner, and D. O. Brien, "Challenges in Wide Coverage Indoor Optical Communications Using Fibre-Wireless-Fibre Links for Terabit data rates," in *IEEE GlobeCom*, 2015.

[22] R. Maher, T. Xu, L. Galdino, M. Sato, A. Alvarado, K. Shi, S. J. Savory, B. C. Thomsen, R. I. Killey, and P. Bayvel, "Spectrally Shaped DP-16QAM Super-Channel Transmission with Multi-Channel Digital Back-Propagation," *Nat. Sci. Reports*, vol. 5, p. 8214, 2015.

[23] F. Chang, K. Onohara, and T. Mizuochi, "Forward error correction for 100 G transport networks," *IEEE Commun. Mag.*, vol. 48, no. 3, pp. 48–55, 2010.

[24] M. Wolf, J. Li, L. Grobe, D. O. Brien, and H. Le Minh, "Challenges in Gbps Wireless Optical Transmission," *Mob. Light. Wirel. Syst.*, vol. 45, pp. 484–495, 2010.

[25] C. X. Xiang Zhou, *Enabling Technologies for High Spectral-efficiency Coherent Optical Communication Networks*, 1st ed. John Wiley & Sons, 2016.

[26] A. Gomez, C. Quintana, G. Faulkner, and D. O'Brien, "Point-to-multipoint holographic beamsteering techniques for indoor optical wireless communications," in *Photonics West*, 2016, vol. 9772, pp. 1–7.

[27] D. Lavery, "Digital Coherent Receivers for Passive Optical Networks," 2013.